

Earth's Future

RESEARCH ARTICLE

10.1029/2020EF001938

Key Points:

- Silicate rock carbon sink is expanded to global scale with high spatial resolution
- There is huge spatial heterogeneity in global silicate rock carbon sink flux
- From 2041 to 2060, silicate rock carbon sink will rise in response to global warming

Supporting Information:

Supporting Information may be found in the online version of this article.

Correspondence to:

X. Bai,
baixiaoyong@vip.skleg.cn


Citation:

Zhang, S., Bai, X., Zhao, C., Tan, Q., Luo, G., Wang, J., et al. (2021). Global CO₂ consumption by silicate rock chemical weathering: Its past and future. *Earth's Future*, 9, e2020EF001938. <https://doi.org/10.1029/2020EF001938>

Received 14 DEC 2020

Accepted 15 APR 2021

Global CO₂ Consumption by Silicate Rock Chemical Weathering: Its Past and Future

Sirui Zhang^{1,2}, Xiaoyong Bai^{2,4,5} , Cuiwei Zhao¹, Qiu Tan¹, Guangjie Luo⁵, Jinfeng Wang^{2,6}, Qin Li^{2,3}, Luhua Wu^{2,3}, Fei Chen^{2,6}, Chaojun Li², Yuanhong Deng^{2,3}, Yujie Yang^{1,2}, and Huipeng Xi^{2,3}

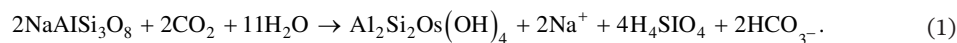
¹School of Geography and Environmental Sciences, Guizhou Normal University, Guiyang, Guizhou Province, China,

²State Key Laboratory of Environmental Geochemistry, Institute of Geochemistry, Chinese Academy of Sciences, Guiyang, China, ³Puding Karst Ecosystem Observation and Research Station, Chinese Academy of Sciences, Guiyang, China, ⁴CAS Center for Excellence in Quaternary Science and Global Change, Xi'an, Shanxi Province, China, ⁵Guizhou Provincial Key Laboratory of Geographic State Monitoring of Watershed, Guizhou Education University, Guiyang, China, ⁶College of Resources and Environmental Engineering, Guizhou University, Guiyang, China

Abstract Silicate rock weathering maintains a stable and long-term absorption of CO₂. However, the magnitude, spatial pattern, and evolution characteristics of global silicate rock weathering carbon sink (SCS) remain unclear. To solve this problem, based on high-precision hydrometeorological data (1996–2017) and CMIP5 data (2041–2060), using the Celine model, we calculated the global silicate rock weathering carbon sink flux (SCSF) magnitude and spatio-temporal distribution for 1996–2017. We also predicted the SCSF under two future greenhouse gas emission scenarios (RCP 4.5 and RCP 8.5). Then, we produced a spatial data set (0.5 × 0.5) of global SCSF from 1996 to 2017 and found that the global average annual SCSF was 1.67 t/km²/yr, and the SCS was 127.11 Tg/yr. In particular, Brazil's silicate rock contribution accounts for nearly a quarter of the global SCS (24.41%). Although the GEM-CO₂ model is now widely used, the SCSF, without considering the temperature, may be overestimated by 5.4%, and the maximum contribution of temperature to it can reach 240 kg/km²/yr. Moreover, the global SCS is now showing a downward trend, but the global emission of greenhouse gases in the future (2041–2060) will continue to increase the carbon sink capacity (23.8%) due to temperature changes. In summary, we have produced a set of high-resolution spatiotemporal data of the past and the future. The above results fill up the large-scale data gap of SCSF and provide a scientific basis for quantitatively assessing the impact of climate change on SCS.

1. Introduction

Silicate carbon sink (SCS) is the net carbon sink that affects the global carbon cycle over a period of millions of years or more (Tao et al., 2011). On the geological time scale, there is a negative feedback mechanism which includes rock weathering, increased CO₂ concentrations, and subsequent environmental changes (Maher & Chamberlain, 2014). Rising CO₂ concentrations leads to periods of global warming, which in turn promote rock weathering, absorbing more CO₂ (Liu et al., 2008, 2011; Xie et al., 2012).



As shown in Equation 1, after the silicate rock is weathered, the primary minerals are decomposed in the river. Then the HCO₃[−] produced by the weathering of silicate rocks is deposited as calcite or dolomite in the ocean. Therefore, the atmospheric CO₂ concentration and global temperature tend to decrease, exerting a long-term control on the global atmospheric CO₂ concentration (Berner et al., 1983; Bolin, 1980; Garrels et al., 1975; Kempe & Degens, 1985; Lenton & Britton, 2006; Walker et al., 1981; Wallmann, 2001). There is no doubt that SCS represents an important part of the global carbon cycle (Caldeira, 1995).

Because of its importance in global carbon cycling, many scientists have carried out research on SCS and made progress toward understanding the related mechanisms. In recent years, two approaches have been taken for exploring SCS: hydrochemical method and simulation modeling. The benefit of studying rivers through the hydrochemical method is that rivers contain most of the dissolved elements of weathered rocks

around the world as they pass through the continental crust and encounter different climatic regions (Gaillardet et al., 1999; Liu & Han, 2020; Veizer & Mackenzie, 2003). After rock weathering, the absorbed CO_2 is converted into soluble ions, such as HCO_3^- , Mg^{2+} , and Ca^{2+} , which enter the river and are transported to the ocean. Therefore, analysis of the relevant ion element contents in a river can be used to quantify the value of CO_2 uptake in its watershed. Gaillardet (1999) calculated the contribution of rainfall, lithology, and atmosphere to rock weathering using the hydrochemical compilation data of 60 major rivers worldwide, and then extended the total amount of carbon in the basin to a global scale based on an inversion model. The resulting estimated worldwide SCS was 0.104 Gt/yr (Gaillardet, 1999). The simulation modeling method has been gradually improved by the development of computer technology in recent decades. Suchet et al. (2003) divided global continental rocks into six types: sand and sandstone, shale, shield rock, acid volcanic rock, basalt, and carbonate rock. They then derived the empirical coefficient digital layer for each rock and combined these data with the constructed GEM- CO_2 model to simulate the global SCS, with a value of 0.155 Gt/yr. Based on previous research, Hartmann (2009) further constructed the “multiplicity of lithology model” and divided continental rocks into 15 categories. This study simulated the consumption of CO_2 by Japanese islands and then converted these data to a global scale through the nonlinear model. It was found that the annual atmospheric CO_2 consumption by the global continental silicate weathering ranged from 0.133 to 0.169 Gt/yr (Hartmann, 2009).

From the results of various studies, it has been observed that the global silicate rock weathering carbon sink flux (SCSF) highly correlates with the rate of silicate weathering (Dessert et al., 2001). In addition, rock weathering carbon sink reflects the complex response of multiple factors, such as runoff (RF) and temperature (T), through the dynamic changes in water chemistry (Berner & Kothavala, 2001; Gislason et al., 2009; Kump et al., 2000; White & Blum, 1995; Zhang, Jiang et al., 2006) and RF is also affected by temperature changes (Gu, 2020). Therefore, carbon sink estimates that ignore temperature in high-temperature regions may not be accurate representations of the actual situation (Godd  ris et al., 2013). Now, there remain large differences and uncertainties in the global SCS (Liao & Zhu, 2010; Moon et al., 2014). To improve the estimates, climate impact factors need to be integrated into global silicate rock calculations. It is worth noting that there is a strong coupling relationship between the chemical weathering and physical erosion of silicate rocks. Although this relationship is important, their internal mechanism and focus are different. Moreover, current chemical models cannot fully reflect the physical processes of erosion and hydrology because it is difficult to accurately identify the effects of physical erosion on large-scale spaces. In conclusion, the magnitude and distribution of SCS also urgently require spatial conversions to produce an accurate output at a spatial resolution of 0.5° and minimize the uncertainty caused by not considering physical erosion (Pu, 2015).

Therefore, this paper quantitatively evaluates the spatial distribution and magnitude of global SCS from 1996 to 2017 at a 0.25° pixel scale while considering the climate impact factors. The aim of this study is to (1) quantify the magnitude of SCS at a global scale, (2) explore the evolution of SCS at a multi-year scale and quantify the contribution of climate factors to its changes, (3) reveal the average carbon sink levels and changes of various countries from 1996 to 2017, and (4) analyze the magnitude and distribution of global SCS under the RCP 4.5 and RCP8.5 greenhouse gas emission scenarios for 2041–2060 as well as clarify the impact of different climate conditions on the SCS. This study is of great importance for improving the carbon cycle model and evaluating SCS, thus providing theoretical support for global environmental governance.

2. Materials and Methods

2.1. Overview

The workflow of the data processing and analysis conducted in this study is shown in Figure 1. First, we used two models to calculate the global silicate rock weathering carbon sink flux.

(SCSF) based on the processed climate data and lithologic data and their SCSFs compared. Subsequently, the SCSF was spatially analyzed to identify the changes from 1996 to 2017. Then, partial derivative method was used to quantify the contribution of temperature and runoff to these changes. Finally, R was used to link these spatial results to specific regions.

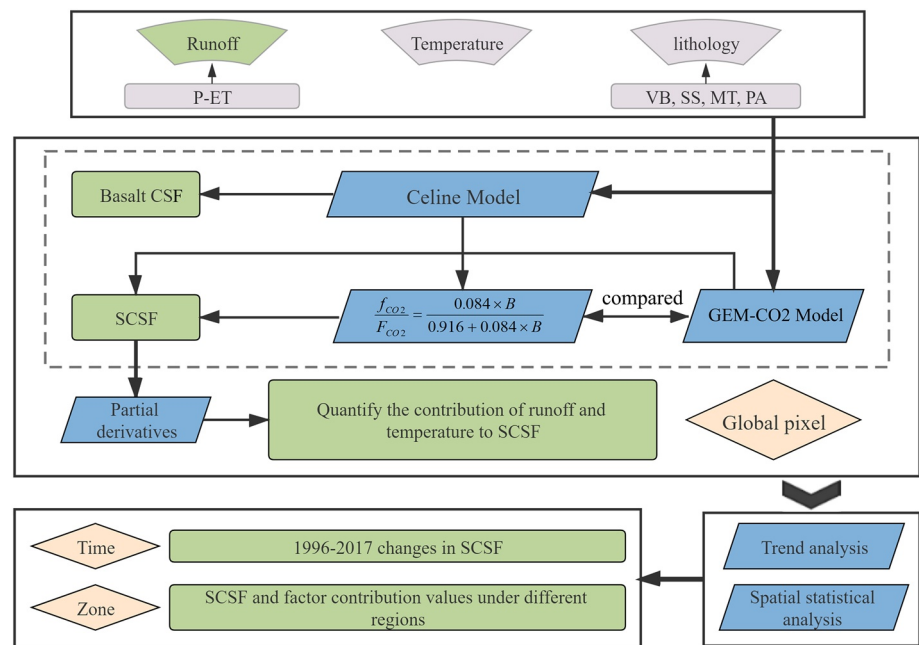


Figure 1. Data and workflow (CSF: carbon sink flux; ET: evaporation; P: precipitation; VB, SS, MT and PA: Basic Volcanic Rocks, Siliciclastic Sediments Rocks, Metamorphic Rocks and Acid Plutonic Rocks; SCSF: silicate rock weathering carbon sink flux).

2.2. Data Sources

First, global-scale meteorological data was derived from global products simulated by the NOAA (0.25×0.25) land-surface process model in the Global Land Data Assimilation System (GLDAS) provided by NASA (Beaudoin & Rodell, 2019; Rodell et al., 2004). According to the precipitation data, monthly scale data were synthesized from these data and converted into monthly rainfall and monthly snowfall based on the number of days in each month, and then the two data were added to the precipitation data in 1996 and 2017. Then, global lithological data were used to fully illustrate the spatial distribution and temporal and spatial evolution of weathered carbon sink in global silicate rocks (Suchet et al., 2003; Hartmann & Moosdorf, 2012; Gong, 2021), including VB, SS, MT and PA (Basic Volcanic Rocks, Siliciclastic Sediments Rocks, Metamorphic Rocks and Acid Plutonic Rocks). Based on global national vector boundaries (<https://gadm.org/>), basin boundaries (<https://grdc.com.au/>), and Köppen climate zone classification data (Finlayson & McMahon, 2007), these results were linked to specific regions by R. Finally, the climate data from 2041 to 2050 were taken from the CMIP5 archive (Coupled Model Intercomparison Project Phase 5) based on the RCP8.5 (Riahi et al., 2007) and medium emission scenario RCP4.5 (Clarke, 2007; Smith & Wigley, 2006; Wise et al., 2009).

2.3. Celine Model

The Celine model (Dessert et al., 2003) selectively used the known river chemistry data of basalt provinces during the rainy and dry seasons in order to estimate the carbon sink flux of basalt weathering. These data were derived from monthly or quarterly sampling for at least 3 years. It focused on studies in areas with large temperature differences in order to observe the effects of runoff. This analysis reveals the correlation between the average atmospheric CO_2 consumption rate, cation weathering rate and silicate weathering rate, and runoff during the sampling period. Therefore, when the runoff was constant, the temperature increased as the observed CO_2 absorption rate increased. This analysis suggests that even under different concentration conditions temperature and precipitation have a major impact on basalt weathering rate and related CO_2 consumption (Dessert et al., 2001; Louvat, 1998; White & Blum, 1995). The formula is derived as follows:

$$f_{CO_2} = R_f \times 323.44 \exp(0.0642T) \times \frac{12}{10^6} \quad (1a)$$

where f_{CO_2} is the basalt absorption rate of CO_2 , R_f , and T represent the runoff (mm) and atmospheric temperature ($^{\circ}C$), respectively. In this paper, we assume runoff is equal to precipitation minus evaporation.

Based on the lithology map (Hartmann & Moosdorf, 2012; Suchet et al., 2003), the model calculated that basalt accounts for 8.4% of the global surface area of silicate rock, so the following formula was used to obtain the ratio of global SCS to the basalt carbon sink:

$$\frac{f_{CO_2}}{F_{CO_2}} = \frac{0.084 \times B}{0.916 + 0.084 \times B} \quad (2)$$

where F_{CO_2} is the global carbon flux of silicate rocks, and B is calculated $B = f_{bas}/f_{sil}$ as (the chemical weathering rate of basalt to the weathering rate of other silicate rocks). According to Dessert et al. (2001), the weathering rate of volcanic rocks is 10 times that of granite and gneiss, and thus the value of B was assigned as 10.

2.4. GEM-CO2 Model

The Global Erosion Model of CO_2 Flux (GEM- CO_2) model is a method for estimating the latitudinal distribution of carbon consumed by global chemical weathering using lithology and continental basin maps (Suchet et al., 2003). The model takes runoff as the main influencing factor of global chemical weathering and obtains the relationship between different lithological weathering rates and runoff, thereby establishing a simple model based on empirical coefficients. By extracting the empirical coefficients of silicate rock types, including basic volcanic rocks (VB), siliciclastic sediment rocks(SS), metamorphic rocks(MT), and acid plutonic rocks(PA), the model can be used to estimate the global SCSF:

$$F_{CO_2} = a \times Q \quad (3)$$

where Q represents the runoff (mm) and a is the empirical coefficient of silicate rock types.

2.5. Trend Analysis

In this study, we analyzed the spatial evolution trend of global SCSF from 1996 to 2017 based on the unitary regression trend analysis method. The calculated slope reflects the trend of the evolution of carbon sink. A slope greater than 0 indicates that the pixel as a whole showed an upward trend during the study period, and otherwise it showed a downward trend. When the slope is equal to zero, the SCS does not change. The magnitude of the slope reflects the magnitude of the increase or decrease of SCSF in the pixel (Zhang et al., 2014). The larger the magnitude of the absolute value of the slope, the greater the change. The calculation formula is as follows:

$$\theta = \frac{n \times \sum_{i=1}^n (i \times CSF_i) - \left(\sum_{i=1}^n i \right) \left(\sum_{i=1}^n CSF_i \right)}{n \times \sum_{i=1}^n i^2 - \left(\sum_{i=1}^n i \right)^2} \quad (4)$$

where θ is the evolution trend, i is the current year, n is the study period, and CSF_i is the weathered carbon sink flux in the i -th year.

2.6. Partial Derivatives for Quantifying the Contribution of Temperature and Runoff Induced SCSF Changes

Roderick (2007) used partial derivatives to evaluate the influence of different factors on the changes of a certain phenomenon. This method has been further expanded and widely used in various fields (Liu & Sun, 2016; Wu et al., 2020; You et al., 2013). From previous studies, we know that in addition to lithology,

SCSF changes mainly depend on RF and T (Dunne, 1978; Guy & Schott, 1989; Meybeck, 1986; Suchet & Probst, 1993; Velbel, 1993; White & Blum, 1995). Therefore, we used Equation 2 to explore the contribution of RF and T to SCSF changes.

$$\frac{dSCSF}{dt} = \frac{\partial SCSF}{\partial X_{RF}} \times \frac{\partial X_{RF}}{dt} + \frac{\partial SCSF}{\partial X_T} \times \frac{\partial X_T}{dt} + \frac{\partial SCSF}{\partial X_a} \times \frac{\partial X_a}{dt} + \frac{\partial SCSF}{\partial X_b} \times \frac{\partial X_b}{dt} \dots + \frac{\partial SCSF}{\partial X_n} \times \frac{\partial X_n}{dt} \quad (5)$$

As shown in formula 5, $\frac{\partial SCSF}{dt}$ represents the trend in which SCSF changes. X_{RF} and X_T represents the change from RF and T to SCSF, and X_a to X_n represent the change of other factors to SCSF. $\frac{\partial Y}{\partial X_{RF}}$, $\frac{\partial Y}{\partial X_T}$... are the partial derivative of the change of SCSF with each factor. Roderick (2007) further explained that each partial derivative can be regarded as their second-order partial correlation coefficient under the elimination of the influence of other variables (Equation 6).

$$R_{xy,z\lambda} = \frac{R_{xy,z} - R_{x\lambda,z} \times R_{y\lambda,x}}{\sqrt{(1 - R_{x\lambda,z}^2) \times (1 - R_{y\lambda,x}^2)}} \quad (6)$$

For ease of understanding, Equation 7 can be viewed as:

$$\frac{dSCSF}{dt} = RF_{CON} + T_{CON} + R_{CON} = \frac{\partial SCSF}{\partial X_{RF}} \times \frac{\partial X_{RF}}{dt} + \frac{\partial SCSF}{\partial X_T} \times \frac{\partial X_T}{dt} + R_{CON} \quad (7)$$

where RF_{CON} is the contribution of RF to SCSF, T_{CON} is the contribution of T to SCSF, and R_{CON} is the contribution of residual factor to SCSF.

2.7. The Analysis of Uncertainty

In the study, several uncertainties needed to be analyzed and quantified. There are two aspects of the uncertainty in our study: (1) The uncertainty of the data: although we used publicly-available data, it is large-scale remote sensing data and we cannot guarantee that every pixel point is consistent with reality. Chen (2008) used three models to evaluate the uncertainty of the global precipitation and surface temperature data and found that the uncertainty for both was less than 1%. Mu (2011) used six methods to calculate the uncertainty of the evapotranspiration data and determined that the uncertainty was 24.35%. (2) The uncertainty of the method: the proportional relationship between basalt and silicate carbon sink has an elastic range of 31%–48% (Dessert et al., 2003), which is an uncertainty of 17%. Thus, we estimated that the uncertainty of our study is 29.71% using the uncertainty model (Landschutzer et al., 2014).

$$\sigma = \sqrt{\sum_{i=1}^n \sigma_i^2} \quad (8)$$

However, the uncertainty does not represent that of the results of this research for each pixel. We think that this value is the accumulation of the uncertainty (i.e., the maximum uncertainty), and it can be expressed as $x \pm y$.

3. Results

3.1. Spatial Distribution Pattern of SCS

3.1.1. Global SCSF Distribution Pattern

The meteorological data for the study period are presented in Figure 2 Regional differences in global evapotranspiration were also apparent (Figure 2a), and the spatial changes were basically consistent with the spatial changes in precipitation. However, the global evaporation was more clearly affected by the distribution of sea and land, and the evaporation gradually decreased from the coast to inland. Global precipitation

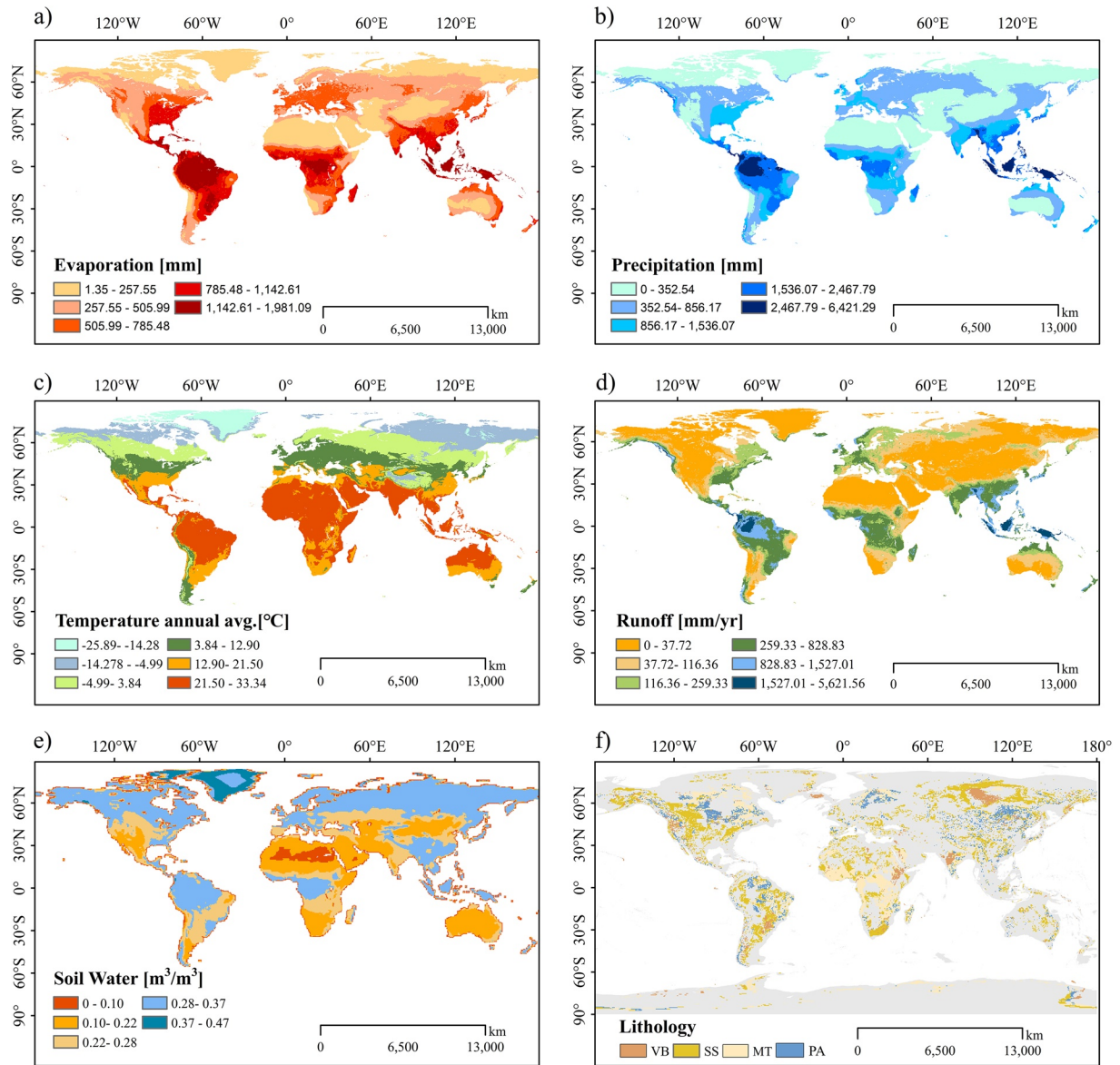


Figure 2. Global distribution of (a) annual average evaporation, (b) annual average precipitation, (c) annual average temperature, (d) annual average discharge, (e) annual average soil water, and (f) silicate rock. (VB, SS, MT, and PA mean basic volcanic rocks, siliciclastic sediment rocks, metamorphic rocks, and acid plutonic rocks, respectively (Gong, 2021; Hartmann & Moosdorf, 2012; Suchet et al., 2003)).

ranged from 0 to 6,421 mm from 1996 to 2017 (Figure 2b), revealing a decreasing spatial trend from the equator to the North and South Poles. The largest precipitation amount was located in the northern part of the South American continent and the coast of Southeast Asia, whereas the African continent near the equator was the largest precipitation region (1,536.07–2,467.79 mm) in the world.

The global average temperature ranged from -25.89°C to 33.34°C (Figure 2c). The spatial distribution trend was highest in the south and lowest in the north. The annual temperature in most regions was above 0°C , accounting for 65.77% of the global area. Areas with an average annual temperature below 0°C were mainly located in northern Eurasia and the Arctic region, among which Greenland's annual minimum temperature fell below -20°C . Areas above 21°C were mainly distributed near the equator, such as northern Australia and Southeast Asia. Affected by the combined effects of precipitation and evaporation, the spatial distribution of runoff (Figure 2d) decreased toward the poles from the equator and decreased inland from the coast. Therefore, high runoff values (1,527–5,621 mm) were mainly concentrated in the coastal areas near the

Table 1
Statistics of Various Lithological Silicate Rock Weathering Carbon Sink Flux (SCSF)

	MT	PA	SS	VB	TOTAL
Area ($\times 10^4$ km ²)	1,924.25	950	2,705.5	578.5	6,165.25
SCSF (t/km ² /yr)	1.98	1.61	1.54	1.35	1.67
SCS (Tg/yr)	47.1	19.12	51.51	9.82	127.11

Abbreviations: VB, SS, MT, and PA mean Basic Volcanic Rocks, Siliciclastic Sediment Rocks, Metamorphic Rocks, and Acid Plutonic Rocks, respectively.

Note. "Area" represents the Area occupied by various lithological SCSF.

equator, coinciding with global high-temperature areas which created favorable conditions for weathering. The global average soil moisture content was between 0 and 0.47 mm³/mm³ (Figure 2e), and each meteorological factor correlated with the global soil moisture relative humidity. The soil water content peaked along the coast of Greenland (0.37–0.47 mm³/mm³). The areas covered by snow and ice throughout the year were characterized by low temperature, low precipitation, and low evaporation.

Based on the global lithological data (Hartmann & Moosdorf, 2012), a global SCSF distribution map (Figure 2f) was drawn and concreted to different lithology. Silicate rocks were divided into four types of lithology (VB, MT, PA, and SS), which occupy an area of about 61.652 million km², accounting for 41% of the global land area. Calculation with Equation 2 estimated the average annual global SCSF over the 1996–2017 period to be 1.67 t/km²/yr, and the distribution characteristics and magnitude of

the carbon sink of different rock types were analyzed in more detail based on the difference of different lithological distributions (Table 1). The annual SCSF of MT, PA, VB, and SS were 1.98, 1.61, 1.35, and 1.54 t/km²/yr, respectively.

There was huge spatial heterogeneity in global SCSF (Figure 3a). The highest value (36.43 t/km²/yr) was located on the Central American Caribbean coast (0°–10°N), but 57.11% of the global SCSF were less than 0.6 t/km²/yr, which was only about a third of the average. Because the global land area was mainly concentrated in the Northern Hemisphere, the global SCSF mainly occurred in the Northern Hemisphere. The global SCSF high-value region was also located in the Northern Hemisphere, which is about 21 times the global average flux. This high value was contributed by MT. In areas with extremely high SCSF, the annual runoff was between 1,527 and 5,621 mm. The natural climate was characterized by high precipitation, high evaporation, high temperature, and high soil water content, which resulted in intensive regional weathering. The central and southern parts of the African continent also had a relatively high SCSF, and the flux (>1.5 t/km²/yr) was higher than the global SCSF. These regions were the major contributors to the global CO₂ consumption of rock weathering.

The global distribution of SCSF was generally concentrated in specific regions based on hydrological conditions and air temperature. However, their impacts on SCSF varied among different geographical locations (Figure 3b). The Central American and Southeast Asian islands had the highest SCSF in the world, being

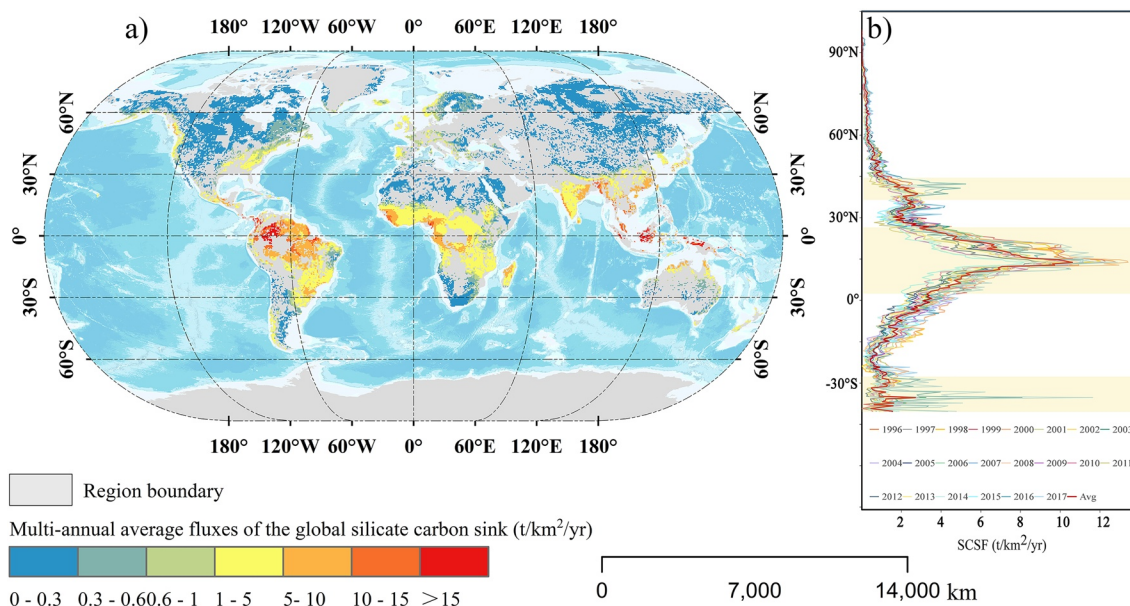


Figure 3. Spatial distribution (a) and latitudinal variation (b) of average annual silicate rock weathering carbon sink flux (SCSF) during 1996–2017.

strongly influenced by high temperature and runoff. This distribution pattern was consistent with the carbon sink flux of carbonate rocks (Bai & Dent, 2009; Li et al., 2016, 2018; Zeng et al., 2017). In the central part of the continent, the high-SCSF areas of the African continent and Australia (>3.0 t/km²/yr) were distributed in areas with high temperature and relatively small runoff, indicating that the impact of temperature was greater than that of runoff. In the middle and high latitudes, although the temperature was low, there was strong precipitation and evaporation in the coastal areas leading to high soil water contents. Subsequently, SCSF was also >3.0 t/km²/yr, indicating that hydrological conditions have a major impact. At high latitudes, although the soil water content was high, the runoff and temperature were low, leading to low SCSF.

3.1.2. Proportion of Silicate Rock Area and CO₂ Consumption in Major River Basins

Table S2 shows the SCSF across the major watersheds worldwide. Because of the zonal influence, the SCSF varied considerably among different watersheds. The top five basins with annual average SCSF were Sepik, Orinoco, Magdalena, Amazon, and Essequibo. Sepik is the main river in northwestern Papua New Guinea, whereas the other four basins are located in South America. Sepik has a tropical rainforest climate, with an average annual temperature of about 21°C–32°C and an average annual rainfall of about 2,500 mm. Although its watershed area is only 1.5×10^3 km², the carbon sink magnitude was as high as 21.59 t/km²/yr, which differed from the second-ranked Orinoco by 5.73 t/km²/yr. The magnitude of SCS in each region during the study period varies widely. For example, Sepik had almost 10 times the global average SCSF; however, the annual average SCS for Sepik was only 0.40 Tg/yr because of the small watershed area. The annual SCSF (2.6 kg/km²/yr) of the Back River located in northern North America was the lowest in the 90 catchments. Moreover, the area of silicate rocks is relatively small, so the total amount is negligible.

Although the SCSF in the Amazon basin was not the highest, the SCS ranked first in the major basins of the world (21.80 Tg/yr), because of the high area of silicate rocks (220×10^4 km²). The top five basins in terms of annual average SCS were Amazon, Zaire (4.46 Tg/yr), Orinoco (3.57 Tg/yr), Parana (2.58 Tg/yr), and Niger (2.06 Tg/yr). The distribution area of silicate rocks in the Amazon, Zaire, Parana, and Niger watersheds were all greater than 1 million km². Although Parana's annual flux was only 3.02 t/km²/yr, its annual average SCS was large because of the large area of silicate rock. The five catchments with the smallest SCS were Olenek, Northern Dvina, Hayes, Back, and Thelon. These rivers are located at high latitude and not only had small fluxes but also small rock distribution areas (total of all rivers: 43.5×10^4 km²). The Mississippi River, which is the important river of the United States, has an area of about 166×10^4 km² but is located at high latitudes where the temperature is relatively low, resulting in a SCSF of only 0.43 t/km²/yr. Its SCS is also at a lower level (0.47 Tg/yr).

3.1.3. SCSF in Different Climatic Zones

The changes in temperature and precipitation indicators were relatively consistent within the same climatic zone, and they are known to be distributed zonally and are closely related to global climate change (B. Li et al., 2016). Therefore, it is important to analyze the global SCSF distribution based on climatic zone. Analysis of silicate rocks in 28 global climate zones revealed that the SCSF and SCS varied significantly among climate zones (Figure 4). The tropical rain forest climate had the greatest CO₂ consumption (12.39 t/km²/yr), which was about 69.03% higher than the tropical monsoon climate, and its SCS accounted for 69.21% of the global total. The potential of SCS in tropical regions was considerable (C. J. Li et al., 2019) under this.

Climatic zone type (characterized by high temperatures throughout the year and long dry seasons), the minimum SCSF also reached 4.24 t/km²/yr (Am). Second, the SCSF in the warm temperate zone was relatively high, with an average of about 2.56 t/km²/yr. The SCSF in the warm zone decreased in the order Cwa (3.12 t/km²/yr), Cwb (2.75 t/km²/yr), Cfa (2.32 t/km²/yr), and Cfb (2.06 t/km²/yr). These climatic zone types (Cwa, Cwb, Cfa, and Cfb) were characterized by high temperatures in summer, and as the latitude increased, their precipitation decreased gradually.

The weathering activity was uneven in the arid zone, but the overall SCS level was low (Arthur et al., 1998) and the SCSF was below 1.5 t/km²/yr. In the arid steppe climate, further refinement of climatic characteristics showed differences in the value of SCSF. Under the same conditions, the hot and dry climate had an SCSF of 1.26 t/km²/yr, which was much larger than the cold and dry climate (0.12 t/km²/yr).

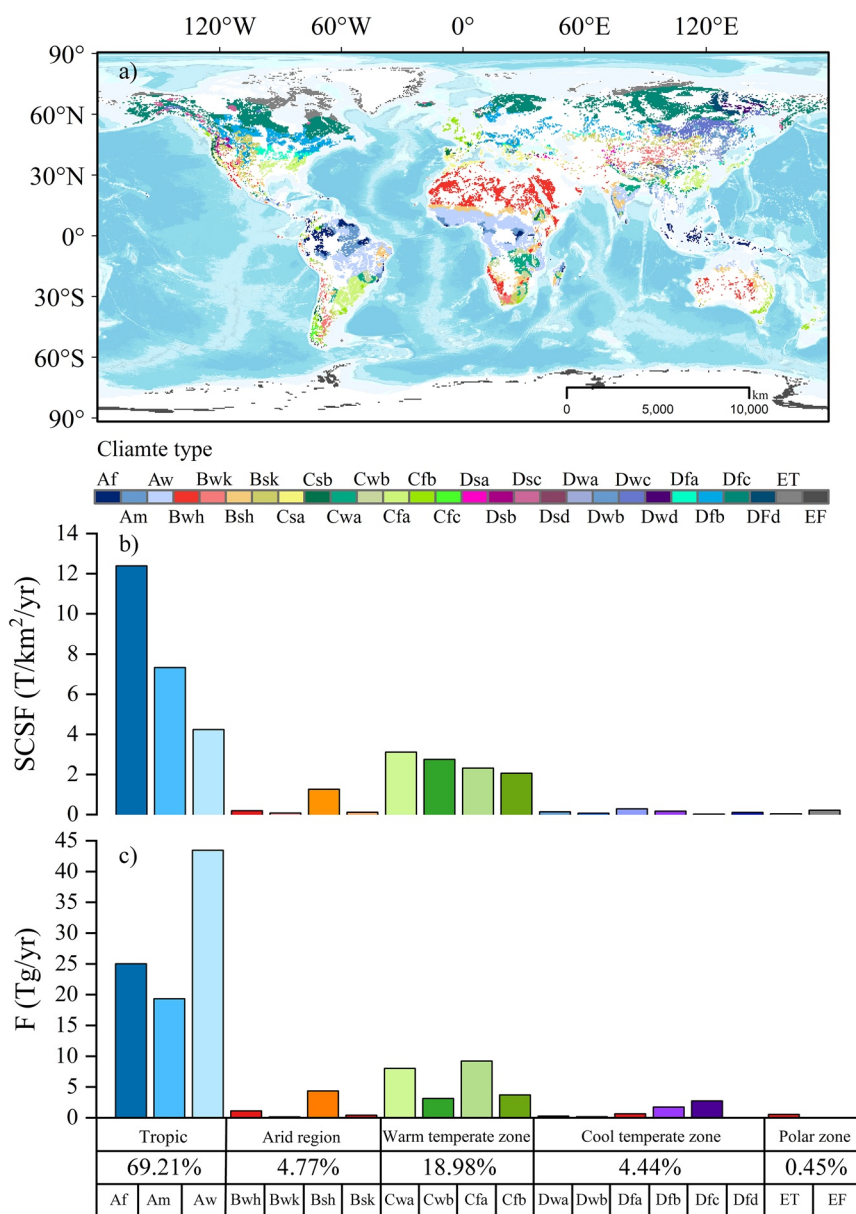


Figure 4. Silicate rock weathering carbon sink flux (SCSF) (b) and silicate rock carbon (SCS) (c) globally based on the Köppen climate classification (a). ((Af) tropical rainforest climate; (Am) tropical monsoon climate; (Aw) tropical dry and wet season climate; (Bwh and Bwk) desert climate; (Bsh and Bsk) semi-arid climate; (Cfa and Cwa) subtropical humid climate; (Cfb, Cwb, Cwc, and Cfc) maritime climate; (Csa and Csb) Mediterranean climate; (Dsa Dfa, Dwa, Dsb, Dfb, and Dw) continental humid climate; (Dfc, Dwc, Dfd, Dwd, Dsc, and Dsd) subpolar climate; (ET and EF) polar climate).

In the cold temperate zone and the polar climate zone, the SCSF was low, and its SCS accounted for the smallest value (0.45%) worldwide. The SCSF fluctuated between 0.04 t/km²/yr and 0.61 t/km²/yr. Relatively, the regions of active silicate rock weathering were mainly concentrated in cold temperate zones with high solar radiation in summer, such as Dwd (0.61 t/km²/yr) and Dfa (0.29 t/km²/yr). The extreme climate zone of inactive silicate rock weathering was mainly distributed in the middle- and high-latitude regions where the coldest month's temperature was below 0°C. In the polar ice cap climate zone in particular, the CO₂ consumption was below 0.05 t/km²/yr.

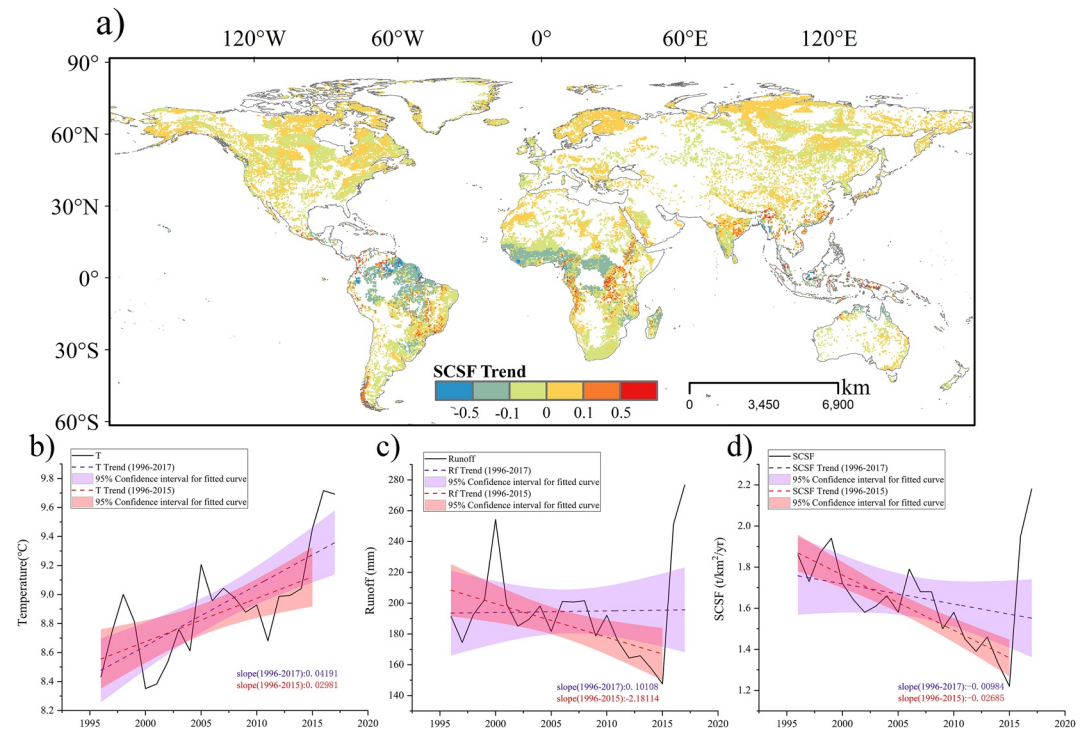


Figure 5. The evolutionary trend of silicate rock weathering carbon sink flux (SCSF) (a) and annual variation of temperature (b), runoff (c), and SCSF (d).

The magnitude and distribution of SCSF was analyzed from the level of latitude as the climate zone decreases from low to high latitudes in the sea and land locations. It was also analyzed from the decreasing levels from coastal to inland locations.

3.2. Past and Future Scenario Simulation of Global SCSF

3.2.1. Trend Analysis of SCSF From 1996 to 2017

During the study period, most of the CO_2 consumption worldwide maintained a constant state and the local SCSF increased only slightly. When segregated by acreage (Figure 5a), the proportions of significant decrease (< -0.5 t/km²/yr), slight decrease (-0.5 to -0.1 t/km²/yr), no change (-0.1 to 0.1 t/km²/yr), slight increase (0.1 – 0.5 t/km²/yr), and significant increase (> 0.5 t/km²/yr) in SCSF were 1.85%, 13.61%, 82.47%, 1.44%, and 0.63%, respectively. The growth areas were mainly concentrated near the western coast of the South Pacific, inland of South Asia, the Indonesian islands of Southeast Asia, northern South America, northeast Africa, and the central west coast. The areas of reduction in SCSF were mainly concentrated in the north west coast of South America. Regardless of the magnitude of the SCSF increase or decrease, tropical regions close to the equator were the regions with the largest interannual variability, ranging from 2.857 to -1.288 t/km²/yr (Figure S1b). And regions with increased and decreased SCSF were often intertwined and geographically adjacent. Figure S1a clearly shows that the areas of largest increase and the largest SCSF decrease worldwide were also mainly concentrated in the tropics. These were Puerto Rico and French Guiana, respectively (Figure 5a). It is worth noting that SCSF in the polar zone did not show obvious changes, but most of its area was still dominated by growth. It accounted for 80% of the entire polar zone. Contrary to the polar zone and the cold temperate zone, although the SCSF in other climatic zones has a larger magnitude and change range, the decline area accounted for a larger proportion, up to 75% (Figure S1).

Temperature and runoff control chemical weathering and dissolution of silicate rocks (H. Li, et al., 2019) and are the key factors of CO_2 absorption, so the global SCSF was also related to sudden changes of these factors in 2016 and 2017. The global temperature change (Figure 5b) maintained a gradual increase from 2015 to 2017, and the global average temperature increased by 0.24°C over these three years. Global warming has

accelerated water cycling and promoted global climate change (Singh, 2017). Coupled with the effects of the El Niño phenomenon, these changes have exacerbated changes in global precipitation, leading to a considerable increase in precipitation in some regions (WMO Statement, 2016; WMO Statement, 2017). Global runoff (Figure 5c) has increased rapidly since 2016. From 2015 to 2017, the global average annual runoff increased by about 128 mm, of which Africa's annual runoff increased by 125 mm on average. The highest flow rate increased from 5,977 to 24,712 mm. From 2016 to 2017, the global SCSF has increased significantly under the influences of high temperature and humidity.

The estimation of SCSF (Figure 5d) showed that from 1996 to 2017 the global annual average SCSF fluctuated and its trend was down. However, since 2016 the global SCSF has suddenly increased sharply, reaching 2.18 t/km²/yr in 2017, and representing a 78.69% increase compared with 2015. The highest value before 2017 was 1.94 t/km²/yr in 1999 and the minimum value (1.22 t/km²/yr) was in 2015. During this period, the average annual reduction was about 0.045 t/km²/yr.

3.2.2. Time Evolution Characteristics of SCS in Different Countries

The SCSF can be used to distinguish between global and national carbon sink functions. We used multi-year mean SCS to analyze the spatio-temporal variation of SCS from 1996 to 2017.

A global time scale analysis was performed on the calculation results of the carbon aggregates, where each arc corresponds to a country reflecting the proportion of the country's SCS (the longer the arc length, the greater the contribution). Each radian corresponding to the time series represents the global SCS during this period. Similarly, the longer the arc length, the greater the total SCS. The connection between the country and time indicates SCS in the area connected during the time period. The wider the connection, the larger the total amount of carbon in that place. Therefore, by analyzing the time series of SCS in detail, the fluctuation of global C consumption on a long-term scale and the extent of carbon sink contribution in different regions in the same period are further intuitively clarified. Based on the global time scale analysis, the global SCS showed significant fluctuations over the study period (Figure 6). Except for 2002 and 2016, the total SCS fluctuated slightly each year. The rate of change of global silicate carbon accumulation showed the trend of the change from less to more. The first three years and the last two years of the study represented the main the growth periods, whereas the middle years hovered around the troughs. In 2002, the total SCS rapidly decreased from 142.42 to 121.09 Tg/yr, a decrease of 15% from the previous year. In 2016, the total SCS soared from 96.97 to 157.09 Tg/yr, representing a 62% increase from the previous year. The global total reached its highest value (157.09 Tg/yr) and its lowest value (96.97 Tg/yr) in 2016–2017 and 2014–2015, respectively. Analysis of the changes in the total SCS within countries reveals that Brazil, Colombia, and India had the largest contribution to carbon sink in the world. The three regions with relatively small contributions were Zambia, Mexico, and Russia; the SCS in the other countries was very small, so this paper did not discuss them. The change in SCS from 1996 to 2017 in most countries was consistent with global fluctuations, the most typical of which was Zambia. The line width between the country and each year fluctuated with the increase and decrease of the radian length of the year, which indicates that the dynamic trend of the carbon sink wave in Zambia was consistent with the global SCS situation. A few countries showed fluctuations that were less consistent with the overall trend. For example, the carbon aggregates of Brazil, Nigeria, Australia, and Madagascar roughly corresponded to global trends, but the maximum values were not in 2016–2017, appearing instead in 2000–2001, 2006–2007, and 1996–1997. Although the SCS for these countries did show an increase in 2016–2017, this increase was relatively low.

3.2.3. SCSF Trends in the Future Scenarios

The Celine model was used to extend the magnitude and spatial distribution of global SCSF to 2041–2060 (Figure 7). Under the RCP8.5 scenario, the global SCSF was estimated as 2.08 t/km²/yr, which will absorb about 158 Tg/yr of CO₂. The SCSF and SCS under the RCP4.5 scenario were estimated as 2.44 t/km²/yr and 170 Tg/yr, respectively. These findings suggest that when CO₂ is emitted at high levels (RCP8.5), SCSF will increase by 24.55% compared with past levels.

Under two different scenarios of greenhouse gas emissions, the estimated overall distribution of annual average SCSF from 2041 to 2060 was similar to that of the past. However, compared with 1996–2017, the SCSF high-value areas are expected to further expand in the future. Areas with SCSF greater than 5 t/km²/yr were found to mainly spread toward the Southern Hemisphere; in particular, the high-SCSF areas of

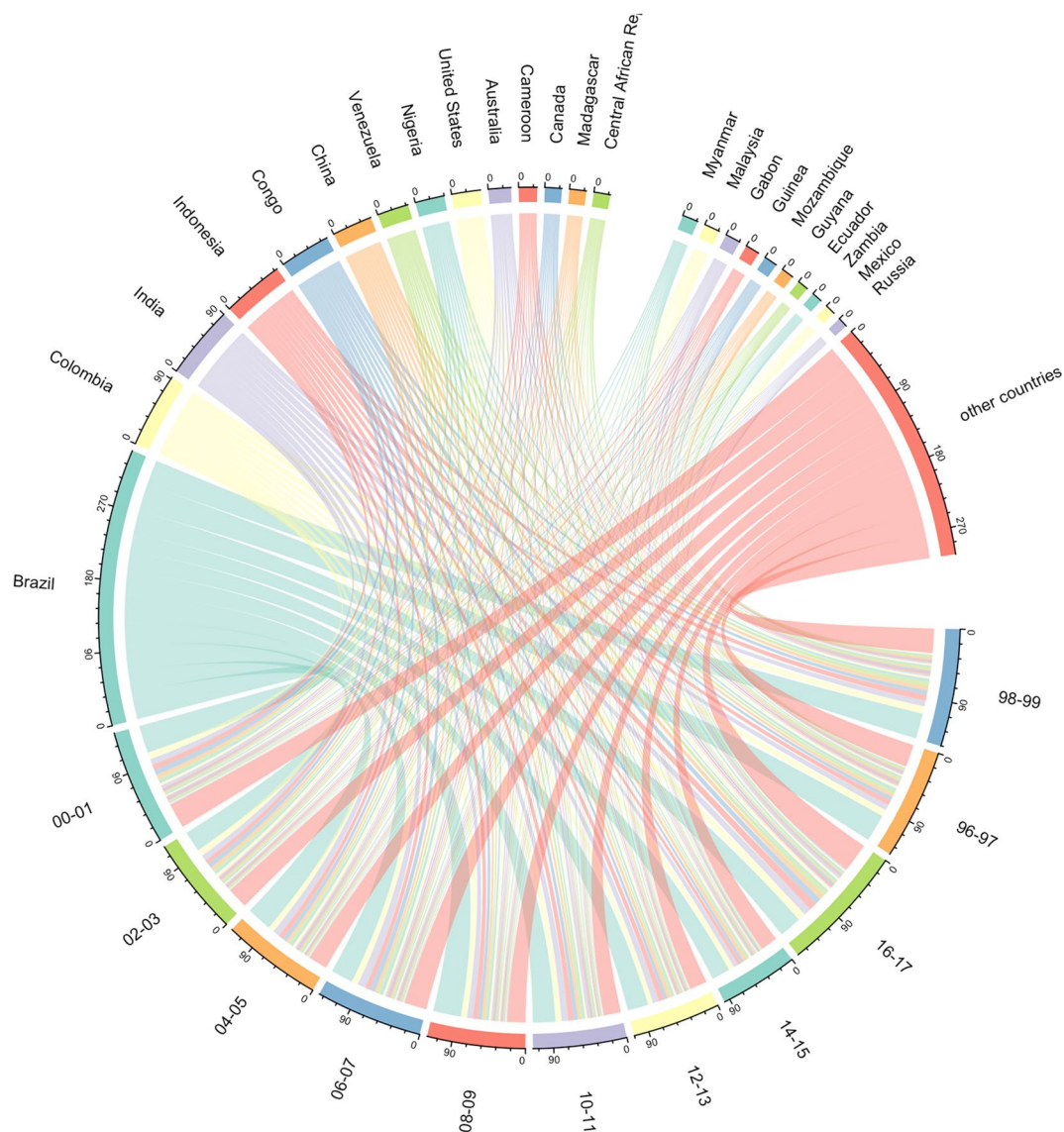


Figure 6. Time evolution map of silicate rocks carbon sink (Tg/yr) from 1996 to 2017.

Australia were predicted to expand from the coast to the inland. South America's SCS capabilities were further enhanced in the future predictions, with average annual SCSFs of 5.14 t/km²/yr (1996–2017), 7.13 t/km²/yr (RCP4.5), and 5.79 t/km²/yr (RCP8.5). In North America, the coastal SCSF also changed from less than 1 t/km²/yr for 1996–2017 to more than 1 t/km²/yr in the future.

Under the RCP4.5 scenario, the growth of global SCSF was predicted to be concentrated in South America, and the SCSF in most areas was predicted to increase toward a trend >5 t/km²/yr. In contrast, the increase at RCP8.5 showed an increase in SCSF in Australia; however, the magnitude of the increase will be less than the former. And because the future temperature rise will further reduce Asia's runoff (Miao, 2020), near 30°N in Asia, the carbon sink of RCP4.5, which is less warm, will be higher than that of RCP8.5.

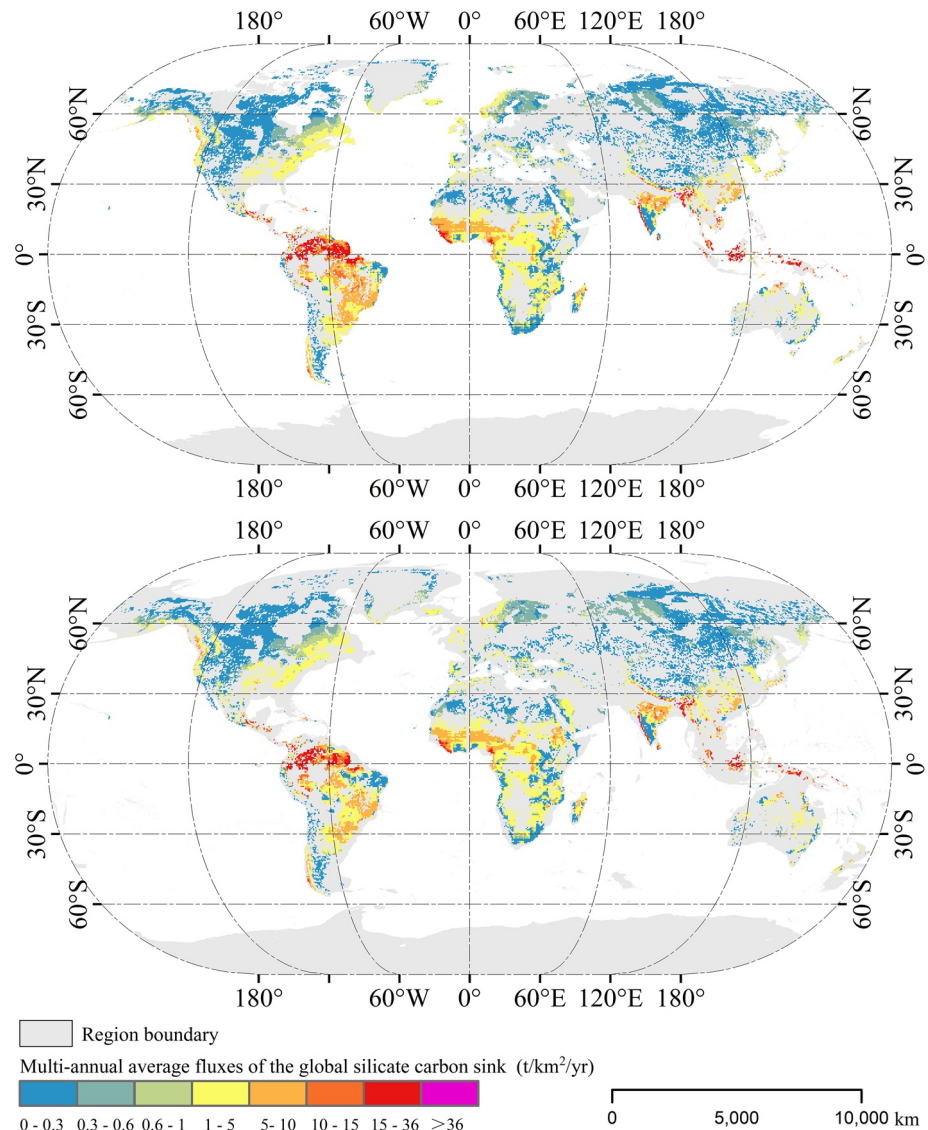


Figure 7. Global SCFS distribution from 2041 to 2060 under the RCP4.5 (a) and RCP8.5 (b) scenarios.

4. Discussion

4.1. Comparison With Other Research Results

In order to further illustrate the reliability of the calculated results, we compare the calculated results with the relevant studies in Table 2. Gaillardet (1999) collected hydrochemical data for 60 major rivers worldwide. After removing atmospheric subsidence input, he calculated the contribution of silicate rock weathering to the dissolved solids of the river, thereby inferring the global surface rock weathering rate and CO_2 consumption. It was estimated that about 0.104 Gt C is absorbed by the chemical weathering of silicate rocks. The calculated values in this paper were considerably higher than these estimates, which may be due to the uncertainty in the distribution area of silicate rocks. Except for the silicate minerals formed in meteorites and moonstones, silicate minerals have almost all diagenesis and mineralization processes in common, regardless of whether they are endogenous, epigenetic, or metamorphic rocks in the crust. For this reason, it is difficult to accurately quantify the exact area of silicate rocks. In addition, the magnitude of global carbon sink is a value that changes continuously with climate, rather than being a constant value. In the period of 1996–2017, the global runoff may be slightly larger, so the calculated value is higher than the value of Gaillardet. So we believe that the method can still be extended to a global scope. Suchet et al. (2003)

Table 2
Comparison of Weathering Carbon Sink of Silicate Rocks Among Different Research Methods

Data	Model	SCSF (t/km ² /yr)	SCS (Tg/yr)	Source
Data for the world's 60 largest rivers	Inversion model	1.28	104	Gaillardet et al. (1999)
Global lithology data	GEM-CO ₂ model	1.32	155	Suchet et al. (2003)
New isotopic data for carbon and sulfur	Global carbon cycle model	1.69	(72 ± 36)–138	Berner (2006)
Spatial geomorphology and climate data	Global geological carbon cycle model	–	150–330	Hilley & Porder. (2008)
Japanese lithology data and sampling site hydrochemical data	Multiplicity of lithology model	–	133–167	Hartmann et al. (2009)
GEMS/Water and HYBAM data	Inversion model	–	69–119	Moon et al. (2014)
Global runoff and temperature data	Celine model	1.67	127	This study

Note. “GEMS/WATER and HYBAM” Represent the United Nations Environmental Program Global Environmental Monitoring System Water Program and the Environmental Research Observatory (ORE) HYBAM (Geodynamical, Hydrological, and Biogeochemical Control of Erosion/Alteration and Material Transport in the Amazon Basin), Respectively.

established the GEM-CO₂ model, and divided the global surface rocks into carbonate rocks, sandstones, shales, acid volcanic rocks, basalts, and ground shields. Based on the layer overlay operation of the model, 0.155 Gt/yr CO₂ consumption of silicate rocks in the global scale was calculated.

According to Suchet's assumption (Suchet et al., 2003), SS, VA, VB, VA, and MT are completely silicate rocks with an area of approximately 116.71×10^6 km². Based on this result, he was deduced that the SCSF obtained in this study was approximately 1.32 t/km²/yr. Because we did not include some igneous rock areas and tectonic activity areas in the current study, so our SCSF value was slightly lower than the calculation results of this model, and the SCS value of this study was also slightly higher than the results of our study. Berner (2006) designed a “global carbon cycle model” using huge computer calculations and estimated the global silicate rock carbon accumulation amount to be 72–138 Tg/yr. Our research results in this paper are within this range, suggesting that our analysis and research on global silicate carbon sink are reasonable. Hilley and Porder (2008) used a model to correlate the flux of a single element with erosion rate, reaction kinetics, weather zone thickness, and dust flux, thereby predicting that silicate weathering would consume 150–330 Tg/yr of CO₂. Hartmann et al. (2009) extrapolated the chemical weathering CO₂ absorption from the Japanese archipelago dominated by silicate rock types to a global scale based on the multiplicity of lithology model framework. The SCSF globally was 133–167 Tg/yr, which is very similar to the results of the current study. Moon et al. (2014) used the bootstrap program and inversion model to derive a new global silicate rock estimate and explain its uncertainty in global rivers. The global CO₂ absorption in this paper was estimated to be 69–119 Tg/yr. The SCS value was similar. Moon (2014) suggested that multiple factors intertwined lead to a certain degree of underestimation of his results because of the uncertainties of climate, flow, and chemical composition in the watershed. The above research results are all similar to the results of our paper. The main reason is that in addition to the uncertainty of the distribution area of silicate rocks, these studies also include the dynamic changes of carbon sink because carbon sink does not have a constant value and is directly related to the local climatic and hydrological conditions. In particular, any rainfall and runoff can induce carbon cycle fluxes (Pu, 2017). Therefore, the inconsistency of research time is also an important factor that causes the little difference in results.

These research data indicate that the research results of this paper are reliable. The model is reasonable and reliable when applied to a global scale, and it is sufficiently accurate to quantify the global magnitude and spatial patterns of SCS.

4.2. Comparison With the GEM-CO₂ Method

The model takes runoff as the main influencing factor of global chemical weathering and obtains the relationship between different lithological weathering rates and runoff, thereby establishing a simple model

based on empirical coefficients. By extracting the empirical coefficients of silicate rock types (PA, VB, SS, and MT), the data can be used to estimate the global SCSF. However, the GEM-CO₂ model only considers the impact of runoff on the weathering rate and thus ignores the comprehensive impact of the environmental background such as temperature, which is closely related to the weathering rate. Moreover, the accuracy of the lithological experience coefficient needs to be improved. There are different degrees of underestimation at the meta-scale. The Celine method in this paper comprehensively considers the global pixel scale evaporation, climate, and surface silicate rock outcrop area, with the purpose of estimating the SCSF more accurately at the pixel scale and clarifying the importance of silicate rock weathering as a geological time-scale net carbon sink within the global carbon cycle.

Table S3 shows the results of this study and the GEM-CO₂ model estimated value for major countries or zones, based on the area of silicate rock from high to low. The SCS and SCSF obtained by GEM-CO₂ were generally similar to the results of this method. The global SCSF using the GEM-CO₂ model and the Celine method obtained were 1.76 and 1.67 t/km²/yr, respectively, and the SCS were 128 and 127 Tg/yr, respectively, indicating that the results from GEM-CO₂ method were slightly higher than those from the Celine method. This may be due to the influence of the climate factors added to the Celine method in this paper. Gaillardet et al. (1999) suggested that the combined effects of runoff and climate can be used to explain the chemical weathering of modern silicate rocks worldwide. Therefore, it is important to include climate factors as a calculation indicator to estimate global SCSF.

Further analysis of the calculation results for different countries and zones under the two models (Table S3) shows that when the annual average temperature of the country (zone) is greater than 25°C, the global SCSF under the two models were very different, and the findings from the Celine model were larger than the GEM-CO₂ data. For example, Benin in West Africa had a difference of 38% among the two studies; the SCSF of the Celine method was 2.69 t/km²/yr, whereas the SCSF obtained by GEM-CO₂ was 1.19 t/km²/yr. Although Benin's annual average runoff was only 260.08 mm, the average annual temperature was as high as 27.37°C. Table S3 shows that the average annual runoff of these countries(zones) with large differences ranges from several hundred millimeters to more than one thousand millimeters; however, their temperatures remained above 25°C. This shows that the weathering rate of silicate rocks was affected more by temperature at annual average temperatures above 22°C and exceeded the effects of runoff and lithology on the SCS. A comparison between Thailand and Taiwan's estimates supports this view. Thailand's average annual runoff was 406.01 mm lower than Taiwan, but the SCSF of Thailand calculated by using the Celine model (6.48 t/km²/yr) was slightly higher than that of Taiwan (6.25 t/km²/yr), probably because its annual average temperature was 6.21°C higher than that of Taiwan. The average annual SCSF of the countries and zone were basically the same. In contrast, the calculation results of GEM-CO₂ showed that the SCSF in Thailand (4.25 t/km²/yr) was much lower than that of Taiwan (8.67 t/km²/yr). Therefore, in regions with high average annual temperatures, the GEM-CO₂ model will seriously underestimate the SCSF, suggesting that this model is unsuitable for this type of environmental area. However, when the average annual temperature is around 10–20°C, the estimated results obtained by the two models were similar. For example, for Zimbabwe located in southeast Africa, the calculation results of the Celine model and GEM-CO₂ were 0.97 and 0.94 t/km²/yr respectively, and the difference between them is only 0.03 t/km²/yr. The average annual temperature of this region, with a tropical grassland climate, was 20.87°C and the annual runoff was 127.16 mm. In this climate, temperature was no longer the main factor affecting the weathering rate of rocks, but the contribution of runoff to the carbon consumption of rock weathering became dominant. Therefore, under these environmental conditions, the results of the method and the GEM-CO₂ model can be generalized to the pixel scale. The SCSF for Russia was inconsistent. The difference between the results of the two models becomes considerable in regions and countries where the average annual temperature was below 10°C. Contrary to the high-temperature environments, under these low-temperature conditions, the calculated values from the Celine model were lower than those of GEM-CO₂, and the calculation result in our paper represents a low estimate. The most typical example is Greenland, which has a cold climate. The calculation results of the two models were 0.094 and 0.394 t/km²/yr, respectively. Greenland has low temperature and low humidity (−17.95°C, 15.66 mm), suggesting an environment with weak weathering. Therefore, the impact of climate on the degree of carbon sink was very low, mainly because of the lithology of the rock itself. Although the difference between the two was 78%, the SCSF was extremely slow in a low-temperature and low-humidity environment. The difference between the results of the two methods is negligible compared

with the global SCSF. Therefore, the Celine model presented in this paper is also suitable for prediction of SCSF in the cold zone. It is worth noting that the SCSF calculated by the two methods was similar in countries where the average annual temperature was around 23°C and the runoff was very low (< 30 mm). For example, the SCSF calculated by the Celine model for Iraq was 0.306 t/km²/yr, whereas the value for GEM-CO₂ was 0.298 t/km²/yr. The difference between the two was only 0.008 t/km²/yr.

4.3. Contributions of RF and *T* to SCSF Change

The contributions of RF and *T* to the changes in the SCSF were quite different (Figure 5). The contribution of RF to the changes in the SCSF was mainly negative (3,149.50 km²), while that of *T* was mainly positive (2,731.25 km²). However, the contribution area and magnitude of *T* were smaller than those of RF. To our surprise, the maximum contribution of RF was a positive contribution (3.20 t/km²/yr), and the maximum contribution of *T* was also a positive contribution.

Contribution (240 kg/km²/yr). As is shown in Figure 8, in the tropical regions of South America and Asia, RF and *T* both played a positive role in the decrease in the SCSF. It should be noted that the opposite was true in tropical Africa. Although RF still had a negative effect, *T* had a greater positive contribution, and to some extent it alleviated the decrease in the SCSF. In the polar zone and cool temperature zone, due to the cold climate, the temperature change during the study period remained relatively constant (Duan et al., 2017; Walsh et al., 2011). Therefore, *T* did not have an effect on the changes in the SCSF (Figure S2c). As far as RF is concerned, in most of the areas in the polar and cool temperature zones, RF had a positive contribution. In the arid region, *T* had a greater positive effect on the changes in the SCSF, but the contribution of RF set off part of the positive contribution of *T*.

As can be seen, RF is the most important factor that influences the changes in the SCSF, and to a certain extent, an increase in *T* can slow down the decrease in the SCSF.

5. Contributions and Shortcomings

5.1. Contributions

In this study, we produced spatial and temporal evolution maps of SCS worldwide, made future spatial predictions, and accurately quantified the magnitude of SCSF at a global scale. The spatial distribution rules

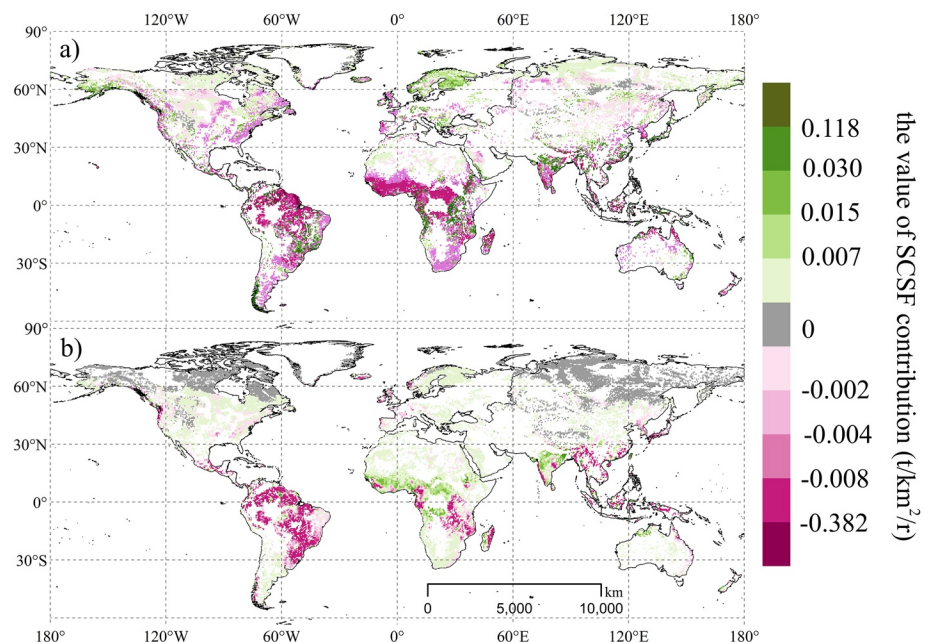


Figure 8. Contribution of runoff (a) and temperature (b) to the spatial variation of silicate rock weathering carbon sink flux (SCSF).

of SCSF under different regional division types and the evolution rules of multi-year scales were clarified. These findings quantify the average SCS levels and changes in countries from 1996 to 2017. The magnitude and distribution of global SCS in the future (2041–2060) were simulated and predicted, and the impact of different climate conditions on carbon sink was illustrated under the RCP4.5 and RCP8.5 scenarios.

5.2. Shortcomings and Limitations

The assumptions in this paper have certain limitations because of the difficulty of obtaining the actual runoff at the pixel scale. Moreover, the areas with a negative runoff depth were ignored, and it was assumed that no weathering of silicate rock takes place. This approach was taken to reduce the deviation of the runoff depth ($RF = P - ET$) derived from calculations from actual results. However, this deviation cannot be completely eliminated, so uncertainty remains about the estimation results, which needs to be improved in future research.

In addition, it should be noted that other environmental factors will also affect the weathering carbon sink of rocks. This article only considers some of these factors, and thus the results obtained in this article are not comprehensive. In the future, relevant factors should be fully considered, such as the effect of human activities and soil CO_2 concentration on SCS and disturbance in the carbon cycle (Jiang, 2018). Moreover, the combination of various factors (e.g., land use and the external effects of interactions between source acids) on the intensity of weathering of rocks should be further explored (Zhang, Xie, et al., 2006).

Finally, the area of silicate rocks is extensive. In order to more accurately quantify the magnitude and distribution of carbon sink in global silicate rocks, it is necessary to further unify the distribution area of silicate rocks and the types of rocks that make up the research results. References have been enhanced.

6. Conclusions

In this study, we used the Celine model to quantify the global spatio-temporal pattern of SCS in the different spatial scales during 2001–2015 and in the future based on high-precision hydrometeorological data (1996–2017) and CMIP5 data (2041–2060). The conclusions are as follows:

- (1) The area of silicate rocks in the world is large ($6,165.25 \times 10^4$ km²), accounting for about 41.38% of the global land area. The SCS was estimated as 127.11 Tg/yr, and the SCSF of silicate rocks was 1.67 t/km²/yr. The annual SCSF for MT, PA, VB, and SS rocks were 1.98, 1.61, 1.35, and 1.54 t/km²/yr, respectively.
- (2) Global SCSF showed huge spatial heterogeneity, for example, 7% of the area of Brazilian silicate rocks contributes to nearly a quarter of the global SCS (24.41%). The highest value (36.43 t/km²/yr) was located in the Central American Caribbean Sea coast (0°–10°N), but 57.11% of the global regional SCSF was less than 0.6 t/km²/yr, only about a third of the average.
- (3) The contributions of RF and T to the changes in the SCSF were quite different. The contribution of RF to the changes in the SCSF was mainly negative (3,149.50 km²), while that of T was mainly positive (2,731.25 km²). However, the contribution area and magnitude of T were smaller than those of RF. As can be seen, RF is the most important factor that influences the changes in the SCSF, and to a certain extent, an increase in T can slow down the decrease in the SCSF.
- (4) Global SCS shows a downward trend. However, the future prediction (2041–2060) suggested an active response of SCS to the global warming trend and its carbon sink capacity was suggested to continue to rise. Moreover, under severe CO_2 emissions (RCP8.5), the global SCSF was predicted to increase by 23.8%, with the growth area concentrated in South America and Australia.

Data Availability Statement

Accesses to all the data sets are as follows: the Global-scale meteorological data set can be downloaded from https://disc.gsfc.nasa.gov/datasets/GLDAS_NOAH025_M_2.1/summary?keywords=GLDAS%20Noah%20Land%20Surface%20Model%20L4%20monthly website. The CMIP5 archive can be downloaded from <http://www.pik-potsdam.de/~mmalte/rcps/index>. The global basins boundaries and national vector boundaries

are available online (<https://grdc.com.au/> and <https://gadm.org>). The global lithological data and Köppen climate zone classification data for this research are included in this paper (and its supplementary information files): [Hartmann, J., & Moosdorf, N. (2012). The new global lithological map database GLiM: A representation of rock properties at the Earth surface. *Geochemistry Geophysics Geosystems*, 13(12). <https://doi.org/10.1594/PANGAEA.788537> Finlayson, B.L., & McMahon, T.A. (2007). Updated world map of the Köppen-Geiger climate classification. *Hydrology and Earth System Sciences*, 11(3):259–263. <https://doi.org/10.5194/hess-11-1633-2007>]. These data sets are available from the data producer upon reasonable request.

Acknowledgments

This research work was supported jointly by the Strategic Priority Research Program of the Chinese Academy of Sciences (No. XDB40000000 & No. XDA23060100), Natural Science Foundation of China (No. 42077455), Western Light Talent Program (Category A) (No. 2018-99), United fund of karst science research center (No. U1612441).

References

- Arthur, M. A., Kump, L. R., Nijjar, R. G., Hotinski, R. M., & Bice, K. L. (1998). When the rivers ran dry: A hypothesis for end-Permian mass extinctions. *Eos, Transactions American Geophysical Union*, 79, F405. <https://doi.org/10.1029/98eo00302>
- Bai, Z., & Dent, D. (2009). Recent land degradation and improvement in China. *AMBIO: A Journal of the Human Environment*, 38, 150–156. <https://doi.org/10.1579/0044-7447-38.3.150>
- Beaudoin, H., & Rodell, M. (2019). *GLDAS Noah Land Surface Model L4 monthly 0.25 x 0.25 degree V2.0, Greenbelt*, Maryland, USA: Goddard Earth Sciences Data and Information Services Center (GES DISC). <https://doi.org/10.5067/9SQ1B3ZXPC5>
- Berner, R. A. (2006). GEOCARBSULF: A combined model for Phanerozoic atmospheric O₂ and CO₂. *Geochimica et Cosmochimica Acta*, 70(23), 5653–5664. <https://doi.org/10.1016/j.gca.2005.11.032>
- Berner, R. A., & Kothavala, Z. (2001). GEOCARB III. A revised model of atmospheric CO₂ over Phanerozoic time. *American Journal of Science*, 294(2), 56–91. <https://doi.org/10.2475/ajs.294.1.56>
- Berner, R. A., Lasaga, A. C., & Garrels, R. M. (1983). The carbonate–silicate geochemical cycle and its effect on atmospheric carbon dioxide over the past 100 million years. *American Journal of Science*, 284(10), 1175–1182. <https://doi.org/10.2475/ajs.284.10.1175>
- Bolin, B., Degens, E. T., Kempe, S., & Ketner, P. (1980). The global carbon cycle — scope. Carbon in the rock cycle. *American Science*, 13.
- Caldeira, K. (1995). Long-term control of atmospheric carbon dioxide; low-temperature seafloor alteration or terrestrial silicate-rock weathering? *American Journal of Science*, 295(9), 1077–1114. <https://doi.org/10.2475/ajs.295.9.1077>
- Chen, M. Y., Shi, W., Xie, P. P., Silva, V. B. S., Kousky, V. E., Higgins, R. W., et al. (2008). Assessing objective techniques for gauge-based analyses of global daily precipitation. *Journal of Geophysical Research*, 113, D04110. <https://doi.org/10.1029/2007JD009132>
- Clarke, L., Edmonds, J., Jacoby, H., Pitcher, H., Reilly, J., & Richels, R. (2007). *Scenarios of greenhouse gas emissions and atmospheric concentrations*. (p. 154). Washington, USA: Sub-report 2.1A of Synthesis and Assessment Product 2.1 by the U.S. Climate Change Science Program and the Subcommittee on Global Change Research, Department of Energy, Office of Biological & Environmental Research.
- Dessert, C., Dupré, B., François, L. M., Schotta, J., Gaillardet, J., Chakrapani, G., et al. (2001). Erosion of deccan traps determined by river geochemistry: Impact on the global climate and the ⁸⁷Sr/⁸⁶Sr ratio of seawater. *Earth and Planetary Science Letters*, 188(2001), 459–474. [https://doi.org/10.1016/S0012-821X\(01\)00317-X](https://doi.org/10.1016/S0012-821X(01)00317-X)
- Dessert, C., Dupré, B., Gaillardet, J., François, L. M., & Allègre, C. J. (2003). Basalt weathering laws and the impact of basalt weathering on the global carbon cycle. *Chemical Geology*, 202(2003), 257–273. <https://doi.org/10.1016/j.chemgeo.2002.10.001>
- Duan, J., Esper, J., Büntgen, U., Li, L., Xoplaki, E., Zhang, H., et al. (2017). Weakening of annual temperature cycle over the Tibetan Plateau since the 1870s. *Nature Communications*, 8, 14008. <https://doi.org/10.1038/ncomms14008>
- Dunne, T. (1978). Rates of chemical denudation of silicate rocks in tropical catchments. evapotranspiration algorithm. *Remote Sens. Environment*, 115, 1781–1800. <https://doi.org/10.1016/j.rse.2011.02.019>
- Finlayson, B. L., & McMahon, T. A. (2007). Updated world map of the Köppen-Geiger climate classification. *Hydrology and Earth System Sciences*, 11(3), 259–263. <https://doi.org/10.5194/hess-11-1633-2007>
- Gaillardet, J., Dupré, B., Louvat, P., & Allègre, C. J. (1999). Global silicate weathering and CO₂ consumption rates deduced from the chemistry of large rivers. *Chemical Geology*, 159(1–4), 3–30. [https://doi.org/10.1016/S0009-2541\(99\)00031-5](https://doi.org/10.1016/S0009-2541(99)00031-5)
- Garrels, R. M., Mackenzie, F. T., & Hunt, C. A. (1975). Chemical cycles and the global environment: Assessing Human Influences. *La Revue Du Praticien*, 37(23), 1321–1325.
- Gislason, S. R., Oelkers, E. H., Eiriksdottir, E. S., Kardjilov, M. I., Gisladóttir, G., Sigfusson, B., et al. (2009). Direct evidence of the feedback between climate and weathering. *Earth and Planetary Science Letters*, 277(1–2), 0–222. <https://doi.org/10.1016/j.epsl.2008.10.018>
- Goddéris, Y., Brantley, S. L., François, L. M., Schott, J., Pollard, D., Déqué, M., & Dury, M. (2013). Rates of consumption of atmospheric CO₂ through the weathering of loess during the next 100 yr of climate change. *Biogeosciences*, 10(1), 135–148. <https://doi.org/10.5194/bg-10-135-2013>
- Gong, S., Wang, S., Bai, X., Luo, G., Wu, L., Chen, F., et al. (2021). Response of the weathering carbon sink in terrestrial rocks to climate variables and ecological restoration in China. *Science of the Total Environment*, 750, 141525. <https://doi.org/10.1016/j.scitotenv.2020.141525>
- Gu, L., Chen, J., Yin, J. B., Xu, C. Y., & Zhou, J. Z. (2020). Responses of precipitation and runoff to climate warming and implications for future drought changes in China. *Earth Future*, 8, e2020EF001718. <https://doi.org/10.1029/2020EF001718>
- Guy, C., & Schott, J. (1989). Multisite surface reaction versus transport control during the hydrolysis of a complex oxide. *Chemical Geology*, 78, 181–204. [https://doi.org/10.1016/0009-2541\(89\)90057-0](https://doi.org/10.1016/0009-2541(89)90057-0)
- Hartmann, J. (2009). Bicarbonate-fluxes and CO₂-consumption by chemical weathering on the Japanese Archipelago — Application of a multilithological model framework. *Chemical Geology*, 265(3–4), 237–271. <https://doi.org/10.1016/j.chemgeo.2009.03.024>
- Hartmann, J., Jansen, N., Dürr, H. H., Kempe, S., & Köhler, P. (2009). Global CO₂-consumption by chemical weathering: What is the contribution of highly active weathering regions. *Global and Planetary Change*, 69(2009), 185–194. <https://doi.org/10.1016/j.gloplacha.2009.07.007>
- Hartmann, J., & Moosdorf, N. (2012). The new global lithological map database GLiM: A representation of rock properties at the Earth surface. *Geochemistry, Geophysics, Geosystems*, 13(12). <https://doi.org/10.1594/PANGAEA.788537>
- Hilley, G. E., & Porder, S. (2008). A framework for predicting global silicate weathering and CO₂ drawdown rates over geologic time-scales. *Proceedings of the National Academy of Sciences*, 105(44), 16855–16859. <https://doi.org/10.1073/pnas.0801462105>

- Jiang, Y. J., Cao, M., Yuan, D. X., Zhang, Y. Z., & He, Q. F. (2018). Hydrogeological characterization and environmental effects of the deteriorating urban karst groundwater in a karst trough valley: Nanshan, SW China. *Hydrogeology Journal*, 26(2018), 1487–1497. <https://doi.org/10.1007/s10040-018-1729-y>
- Kempe, S., & Degens, E. T. (1985). An early soda ocean? *Chemical Geology*, 53(1), 95–108. [https://doi.org/10.1016/0009-2541\(85\)90023-3](https://doi.org/10.1016/0009-2541(85)90023-3)
- Kump, L. R., Brantley, S. L., & Arthur, M. A. (2000). Chemical weathering, Atmospheric CO₂, and climate. *Annual Review of Earth and Planetary Sciences*, 28, 611–667. <https://doi.org/10.1146/annurev.earth.28.1.611>
- Landschützer, P., Gruber, N., Bakker, D. C. E., & Schuster, U. (2014). Recent variability of the global ocean carbon sink. *Global Biogeochemical Cycles*, 28, 927–949. <https://doi.org/10.1002/2014GB004853>
- Lenton, T. M., & Britton, C. (2006). Enhanced carbonate and silicate weathering accelerates recovery from fossil fuel CO₂ perturbations. *Global Biogeochemical Cycles*, 20, GB3009. <https://doi.org/10.1029/2005GB002678>
- Li, B., Gasser, T., Ciais, P., Piao, S., Tao, S., Balkanski, Y., et al. (2016). The contribution of China's emissions to global climate forcing. *Nature*, 531, 357–361. <https://doi.org/10.1038/nature17165>
- Li, C. J., Wang, S. J., Bai, X. Y., Tan, Q., Li, H. W., Li, Q., et al. (2019). Assessment of carbonate weathered carbon sink in major global river basins. *Journal of Geographical Sciences*, 74(07), 1319–1332. Retrieved from <http://www.geog.com.cn/CN/10.11821/dlxb201907004>
- Li, H., Wang, S., Bai, X., Cao, Y., & Wu, L. (2019). Spatiotemporal evolution of carbon sequestration of limestone weathering in China. *Science China Earth Sciences*, 62, 974–991. <https://doi.org/10.1007/s11430-018-9324-2>
- Li, H., Wang, S., Bai, X., Luo, W., Tang, H., Cao, Y., et al. (2018). Spatiotemporal distribution and national measurement of the global carbonate carbon sink. *The Science of the Total Environment*, 643(2018), 157–170. <https://doi.org/10.1016/j.scitotenv.2018.06.196>
- Li, Y., Bai, X., Zhou, Y., Qin, L., Tian, X., Tian, Y., & Li, P. (2016). Spatial-temporal evolution of soil erosion in a typical mountainous Karst Basin in SW China, based on GIS and RUSLE. *Arabian Journal for Science and Engineering*, 41, 209–221. <https://doi.org/10.1007/s13369-015-1742-6>
- Liao, H., & Zhu, Y. D. (2010). Global carbon cycle and climate change in China over the past century. *Quaternary Sciences*, 30(3), 445–455. <http://www.dsjy.com.cn/CN/Y2010/V30/I3/445>
- Liu, C. Q., Jiang, Y. K., Tao, F. X., Lang, Y. C., & Li, S. L. (2008). Chemical weathering of carbonate rocks by sulfuric acid and the carbon cycling in Southwest China. *Geochimica et Cosmochimica Acta*, 37(4), 404–414. <https://doi.org/10.3321/j.issn:0379-1726.2008.04.014>
- Liu, J., & Han, G. (2020). Effects of chemical weathering and CO₂ outgassing on $\delta^{13}\text{C}_{\text{DIC}}$ signals in a karst watershed. *Journal of Hydrology*, 589, 125192. <https://doi.org/10.1016/j.jhydrol.2020.125192>
- Liu, W., & Sun, F. (2016). Assessing estimates of evaporative demand in climate models using observed pan evaporation over China. *Journal of Geophysical Research - D: Atmospheres*, 121, 8329–8349. <https://doi.org/10.1002/2016JD025166>
- Liu, Z., Dreybrodt, W., & Liu, H. (2011). Atmospheric CO₂ sink: Silicate weathering or carbonate weathering. *Quaternary science*, 31, 426–430. <https://doi.org/10.1016/j.apgeochem.2011.03.085>
- Louvat, P., & Allègre, C. J. (1998). Riverine erosion rates on Sao Miguel volcanic island, Azores archipelago. *Chemical Geology*, 148(3–4), 177–200. [https://doi.org/10.1016/S0009-2541\(98\)00028-X](https://doi.org/10.1016/S0009-2541(98)00028-X)
- Maher, K., & Chamberlain, C. P. (2014). Hydrologic regulation of chemical weathering and the geologic carbon cycle. *Science*, 343(6178), 1502–1504. <https://doi.org/10.1126/science.1250770>
- Meybeck, M. (1986). Composition chimique des ruisseaux non pollués en France. Chemical composition of headwater streams in France. *Smart Geo Layers*, 39, 3–77. <https://doi.org/10.3406/sgeol.1986.1719>
- Miao, L. J., Li, S. Y., Zhang, F., Chen, T. X., Shan, Y. P., & Zhang, Y. S. (2020). Future drought in the dry lands of Asia under the 1.5 and 2.0 degrees C warming scenarios. *Earth Future*, 8, e2019EF001337. <https://doi.org/10.1029/2019EF001337>
- Moon, S., Chamberlain, C. P., & Hilley, G. E. (2014). New estimates of silicate weathering rates and their uncertainties in global rivers. *Geochimica et Cosmochimica Acta*, 134, 257–274. <http://dx.doi.org/10.1016/j.gca.2014.02.033>
- Mu, Q. Z., Zhao, M. S., & Running, S. W. (2011). Improvements to a MODIS global terrestrial. *Nature*, 274, 244–246. <https://doi.org/10.1038/274244a0>
- Pu, J. B., Jiang, Z. C., Yuan, D. X., & Zhang, C. (2015). Some opinions on rock-weathering-related carbon sink from the IPCC fifth assessment report. *Advances in Earth Science*, 30(10), 1081–1090. Retrieved from <http://www.adearth.ac.cn/CN/10.11867/j.issn.1001-8166.2015.10.1081>
- Pu, J. B., Liu, W., Jiang, G. H., & Zhang, C. (2017). Karst dissolution rate and implication under the impact of rainfall in a typical subtropic karst dynamic system: A strontium isotope method. *Geological Review*, 63(1), 165–176. <https://doi.org/10.16509/j.georeview.2017.01.015>
- Riashi, K., Grübler, A., & Nakicenovic, N. (2007). Scenarios of long-term socio-economic and environmental development under climate stabilization. *Technological Forecasting and Social Change*, 74(7), 887–935. <https://doi.org/10.1016/j.techfore.2006.05.026>
- Rodell, M., Houser, P. R., Jambor, U., Gottschalk, J., Mitchell, K., Meng, C.-J., et al. (2004). The global land data assimilation system. *Bulletin of the American Meteorological Society*, 85, 381–394. https://doi.org/10.1007/978-94-010-0029-1_30
- Roderick, M. L., Rotstain, L. D., Farquhar, G. D., & Hobbins, M. T. (2007). On the attribution of changing pan evaporation. *Geophysical Research Letters*, 34, L17403. <https://doi.org/10.1029/2007GL031166>
- Singh, F. P. (2017). Global climate change: The present scenario. *American Journal of Life Sciences. Special Issue: Environmental Toxicology*, 5, 10–14. <https://doi.org/10.11648/j.ajls.s.2017050301.12>
- Smith, S. J., & Wigley, T. M. L. (2006). Multi-gas forcing stabilization with the MiniCAM. *Energy Journal*, 3, 373–391. Retrieved from <https://www.jstor.org/stable/23297091>
- Suchet, P. A., & Probst, J. L. (1993). Modelling of atmospheric CO₂ consumption by chemical weathering of rocks: Application to the Garonne, Congo and Amazon basins. *Chemical Geology*, 107, 205–210. [https://doi.org/10.1016/0009-2541\(93\)90174-H](https://doi.org/10.1016/0009-2541(93)90174-H)
- Suchet, P. A., Probst, J. L., & Ludwig, W. (2003). Worldwide distribution of continental rock lithology: Implications for the atmospheric/soil CO₂ uptake by continental weathering and alkalinity river transport to the oceans. *Global Biogeochemical Cycles*, 17(2), 1038. <https://doi.org/10.1029/2002GB001891>
- Tao, Z., Gao, Q., & Liu, K. (2011). Carbon sequestration capacity of the chemical weathering processes within drainage basins. *Quaternary Sciences*, 31(3), 408–416. <https://doi.org/10.3969/j.issn.1001-7410.2011.03.02>
- Veizer, J., & Mackenzie, F. T. (2003). Evolution of sedimentary rocks. *Treatise on Geochemistry*, 271(1551), 369–407. <https://doi.org/10.1016/B0-08-043751-6/07103-6>
- Velbel, M. A. (1993). Temperature dependence of silicate weathering in nature: how strong a negative feedback on long-term accumulation of atmospheric CO₂ and global greenhouse warming? *Geology*, 21, 1059–1062. [https://doi.org/10.1130/0091-7613\(1993\)021](https://doi.org/10.1130/0091-7613(1993)021)
- Walker, J. C. G., Hays, P. B., & Kasting, J. F. (1981). A negative feedback mechanism for the long-term stabilization of Earth's surface temperature. *Journal of Geophysical Research*, 86(C10), 9776–9782. <https://doi.org/10.1029/JC086iC10p09776>

- Wallmann, K. (2001). Controls on the cretaceous and cenozoic evolution of seawater composition, atmospheric CO₂ and climate. *Geochimica et Cosmochimica Acta*, 65, 3005–3025. [https://doi.org/10.1016/S0016-7037\(01\)00638-X](https://doi.org/10.1016/S0016-7037(01)00638-X)
- Walsh, J. E., Overland, J. E., Groisman, P. Y., & Rudolf, B. (2011). Ongoing climate change in the Arctic. *Ambio*, 40, 6–16. <https://doi.org/10.1007/s13280-011-0211-z>
- White, A. F., & Blum, A. E. (1995). Effects of climate on chemical weathering in watersheds. *Geochimica et Cosmochimica Acta*, 59(9), 1729–1747. [https://doi.org/10.1016/0016-7037\(95\)00078-E](https://doi.org/10.1016/0016-7037(95)00078-E)
- Wise, M., Calvin, K., Thomson, A., Clarke, L., Bond-Lamberty, B., Sands, R., et al. (2009). Implications of limiting CO₂ concentrations for land use and energy. *Science*, 324, 1183–1186. <https://science.sciencemag.org/content/324/5931/1183>
- WMO Statement on the state of the global climate. (2016). Retrieved from https://library.wmo.int/index.php?lvl=notice_display&id=19835/ accessed 19 Feb. 2020.
- WMO Statement on the state of the global climate. (2017). Retrieved from https://library.wmo.int/index.php?lvl=notice_display&id=20220#.Xk0yvtPjw3k/ accessed 19 Feb. 2020.
- Wu, L. H., Wang, S. J., Bai, X. Y., Tian, Y. C., Luo, G. J., Wang, J. F., et al. (2020). Climate change weakens the positive effect of human activities on karst vegetation productivity restoration in southern China. *Ecological Indicators*, 115, 106392. <https://doi.org/10.1016/j.ecolind.2020.106392>
- Xie, C., Gao, Q., & Tao, Z. (2012). Reviewed and perspectives of the study on chemical weathering and hydro-chemistry in river basin. *Tropical Geography*, 32(04), 331–337. Retrieved from <http://www.rddl.com.cn/CN/Y2012/V32/I04/331>
- You, G., Zhang, Y., Liu, Y., Song, Q., Lu, Z., Tan, Z., et al. (2013). On the attribution of changing pan evaporation in a nature reserve in SW China. *Hydrological Processes*, 27, 2676–2682. <https://doi.org/10.1002/hyp.9394>
- Zeng, C., Wang, S. J., Bai, X. Y., Li, Y. B., Tian, Y. C., Li, Y., et al. (2017). Soil erosion evolution and spatial correlation analysis in a typical karst geomorphology, using RUSLE with GIS. *Solid Earth Discussions*, 8, 721–736. <https://doi.org/10.5194/se-8-721-2017>
- Zhang, C., Jiang, Z. C., He, S. Y., Jiang, Y. J., Li, L. L., & Wang, J. L. (2006). The karst dynamic system of vertical zoned climate region: A case study of the Jinpo Mountain state nature reserve in Chongqing. *Acta Geoscientia Sinica*, 27(5), 510–514. <https://doi.org/10.3975/cagsb.2006.05.14>
- Zhang, C., Xie, Y. Q., Lv, Y., Jiang, Y. J., Cao, J. H., & Jiang, G. H. (2006). Impact of land-use patterns upon karst processes: Taking Nongla Fengcong depression area in Guangxi as an example. *Acta Geographica Sinica*, 61(11), 1181–1188. <https://doi.org/10.11821/xb200611007>
- Zhang, J., Zhang, L., Xu, C., Liu, W., Qi, Y., & Wo, X. (2014). Vegetation variation of mid-subtropical forest based on MODIS NDVI data - A case study of Jinggangshan City, Jiangxi Province. *Acta Ecologica Sinica*, 34, 7–12. <https://doi.org/10.1016/j.chnaes.2013.09.005>